Atmospheric
Chemistry
and Physics
Discussions

Open Access

Evolution of gaseous precursors and meteorological parameters during new particle formation events in the Central European boundary layer

J. Größ[1], W. Birmili[1], A. Hamed[1,2,†], A. Sonntag[1], A. Wiedensohler[1], G. Spindler[1], H. E. Maninnen[3], T. Nieminen[3], M. Kulmala[3], U. Hõrrak[4], and C. Plass-Dülmer[5]

[1]Leibniz Institute for Tropospheric Research, Permoserstrasse 15, 04 318 Leipzig, Germany
[2]Department of Applied Physics, University of Eastern Finland, P.O. Box 1627, 70211 Kuopio, Finland
[3]Department of Physics, University of Helsinki, P.O. Box 64, 00014 Helsinki, Finland
[4]Institute of Physics, University of Tartu, Ülikooli 18, 50090 Tartu, Estonia
[5]German Meteorological Service DWD, Albin-Schwaiger-Weg 10, 82383 Hohenpeissenberg, Germany
[†]deceased

Title Page

Abstract | Introduction

Conclusions | References

Tables | Figures

|◄ | ►|

◄ | ►

Back | Close

Full Screen / Esc

Printer-friendly Version

Interactive Discussion

Title Page

Abstract   Introduction

Conclusions   References

Tables   Figures

◀   ▶

◀   ▶

Back   Close

Full Screen / Esc

Printer-friendly Version

Interactive Discussion

Abstract

This paper revisits the atmospheric new particle formation (NPF) process in the polluted Central European troposphere, focusing on the diurnal evolution of the meteorological and gas phase parameters involved. Atmospheric aerosol observations include Neutral cluster and Air Ion Spectrometer (NAIS) measurements at the research station Melpitz, East Germany between 2008 and 2011. Particle formation events were classified by a new automated method based on the convolution integral of particle number concentration in the diameter range 2–20 nm. To study the relationship with gaseous precursors, a proximity measure was calculated for the sulfuric acid concentration on the basis of a one month intensive measurement campaign in May 2008. A major result was that the number concentration of fresh produced neutral particles correlated significantly with the amount of sulfur dioxide available as a main precursor of sulfuric acid. The condensation sink, a factor potentially inhibiting NPF events, played a subordinate role only. The same held for experimentally determined ammonia concentrations, which also represent a recognised precursor of aerosol particle nucleation. The analysis of meteorological parameters confirmed the absolute need for solar radiation to induce NPF events, and demonstrated the presence of significant turbulence during those events. Due to its tight correlation with solar radiation, however, an independent effect of turbulence for NPF could not be established with certainty. On the basis of observed diurnal cycles of aerosol, gas phase, and meteorological parameters near the ground, we conclude that particle formation is likely to be induced aloft, rather than near the ground.

1 Introduction

Atmospheric aerosol particles have been recognized as one of the major uncertainties in predicting atmospheric radiative forcing and, thus, future climate (IPCC, 2013). As a first effect, aerosol particles influence the Earth's radiation balance by scattering and

absorbing solar radiation directly (Haywood and Boucher, 2000). Second, aerosol particles act as cloud condensation nuclei (CCN) and thus modify the radiative properties of cloud droplets in various ways (Lohmann and Feichter, 2005). The most influential aerosol effects are thought to be those related to changes in terrestrial temperature and precipitation patterns. Besides climate, atmospheric aerosol particles play a crucial role in the assessment of air quality and their adverse effects upon human health (Pope and Dockery, 2006). Due to the complex interactions involved in the life-cycle of aerosol particles, research work has started to follow a highly integrated approach to elucidate aerosol climate effects across the different time and length scales relevant in the atmosphere (Kulmala et al., 2011).

Nucleation of aerosol particles from gaseous precursors is one of the most important sources of atmospheric particle number. The formation of new aerosol particles in the atmosphere has been shown to occur in almost any atmospheric environment around the world (Weber et al., 1999; Kulmala et al., 2004; Jeong et al., 2010). Considerable efforts have been achieved to make the smallest atmospheric particles (around 1 nm in diameter), and some of their properties visible by instrumentation (Sipilä et al., 2014). The body of atmospheric and laboratory studies have clearly identified sulfuric acid as a key precursor for atmospheric particle nucleation (Paasonen et al., 2010), although the nucleation rates obtained from field and laboratory observations have been reconciled only recently (Sipilä et al., 2010). Laboratory work suggests that the acid-base interaction, such as found between sulphuric acid and ammonia, may play a crucial role in the stabilisation of molecular clusters under conditions relevant for the troposphere (Schobesberger et al., 2014; Almeida et al., 2013). Important open questions prevail, for example, with respect to the relevance of ion-induced formation and growth (Manninen et al., 2010; Yu and Turco, 2011), or an involvement of organic molecules in the nucleation process (Riccobono et al., 2014). Several works strongly suggested to look at the atmospheric particle formation process from a micrometeorological perspective, including the role of turbulent fluctuations (Easter and Peters, 1994; Nilsson

et al., 2001), albeit these ideas have not further substantiated, e.g., in the shape of widely applicable models.

The lifetime of the freshly formed particles and thus, their chance to make further impact on the radiative balance and the budged of CCN (cloud condensation nuclei) depends, however, crucially on their ability to grow to larger diameters. Only rapid growth by condensation can prevent the particles from being lost by coagulation with bigger particles (Kerminen and Kulmala, 2002; Riipinen et al., 2011). An assessment of the climate effects induced by atmospheric nucleation thus requires accurate descriptions of the nucleation process itself (on a molecular level), and the subsequent growth of the nucleation mode into Aitken and accumulation mode particles. For computational reasons, large-scale atmospheric models usually depend on parameterizations of particle nucleation and growth processes (Spracklen et al., 2010). Overall, the degree to which particle nucleation is actually able to influence the budget of CCNs and thus terrestrial climate has, to date, to be considered highly uncertain (Kerminen et al., 2012).

Melpitz is an atmospheric research station in East Germany where new particle formation events have been studied since 1996 (Birmili and Wiedensohler, 2000; Birmili et al., 2001). The frequency of new particle formation events at Melpitz tend to be high during the spring, summer and autumn, with daily frequencies ranging between 30 and 50 % in those seasons (Hamed et al., 2010). The average particle formation and growth rates of particles in the size range of 3–11 nm were estimated as $\sim 10\,\mathrm{cm}^{-3}\,\mathrm{s}^{-1}$ and $\sim 4\,\mathrm{nm}\,\mathrm{h}^{-1}$, respectively (Birmili and Wiedensohler, 2000), and fall within the range spanned by observations in the continental boundary layer. Wehner et al. (2005) emphasised that sulphuric acid alone is by far not sufficient to explain the subsequent growth of the nucleation mode particles. Hamed et al. (2010) suggested a connection between the observed decreasing trends in the concentration of anthropogenic SO_2 (−65 %), the frequency of NPF events (−45 %), and the particle formation rates formation rates (−68 %) between 1996 and 2006. Conversely, the growth rates of nucleated particles apparently have increased (+22 %) over that period. The converse trends in

particle formation and growth rates point to an independence of the chemical species responsible for these two processes.

This paper revisits atmospheric new particle formation at Melpitz with a novel data set collected between 2008 and 2011. Neutral cluster and air ion spectrometers (NAIS) were used to detect aerosol particles from 2 nm in size and at higher time resolution than previously available. For a total of 269 observation days, we examined correlations between new particle formation events, calculated proximity measures for gaseous precursors and ternary nucleation rates, and meteorological parameters including small-scale turbulence.

2 Methods

2.1 The research station in Melpitz

Measurements of nucleation mode particles and particle number size distributions were performed from 2008 to 2011 at the atmospheric research station in Melpitz, Eastern Germany (51°32′ N; 12°54′ E; 87 m a.s.l.). The station is surrounded by flat grass lands, agricultural pastures and woodlands within several tens of kilometers, and neither obstacles nor larger sources of pollution lie within the immediate vicinity of the station. The Melpitz station is a part of the observation networks German Ultrafine Aerosol Network (GUAN; Birmili et al., 2009) and ACTRIS (Aerosols, clouds, and trace gases research Infrastructure network). Atmospheric particle size distributions, measured at Melpitz station, can be regarded as representative of regional background conditions in Central Europe (Asmi et al., 2011). For the basic features of particle number size distributions and particle mass concentrations as a function of meteorological parameters, see Engler et al. (2007) and Spindler et al. (2010).

2.2 Instrumentation

Particle number size distributions were measured using three independent particle size spectrometers: Neutral Cluster and Air Ion Spectrometer (NAIS), mobility diameters 0.75–45 nm; Twin Differential Mobility Particle Size Spectrometer (TDMPS), mobility diameters 3–800 nm; Aerodynamic Particle Size Spectrometer (APS), aerodynamic diameters 0.5–10 µm. Using these instruments, a total of four coherent measurement periods were covered (see Table 1).

2.2.1 Neutral Cluster and Air Ion Spectrometer (NAIS)

The Neutral Cluster and Air Ion Spectrometer (NAIS) is an extended version of the Air Ion Spectrometer (AIS). The NAIS can measure the mobility distribution of ions plus the size distribution of neutral particles, while the AIS is only able to detect ions. For the state-of-the-art of this instrument, see Mirme and Mirme (2013). Briefly, the NAIS uses a charging-filtering section in order to measure particles that are neutrally charged in the atmosphere. The aerosol sample passes first through a unipolar corona charger. Then, the charged particles are classified in the multichannel differential mobility analyser with the electric current carried by the particles being recorded by individual electrometrical amplifiers. The charged fraction of particles induced in the aerosol sample is estimated from the Fuchs theory (Fuchs and Sutugin, 1971). The corona ions generated in the unipolar charger are generally small (< 2 nm), with their exact size depending on concentration, air composition, polarity, and other factors related to particle charging (Manninen et al., 2011). The small excess corona ions are removed by electrical filters, and leave an instrumental size range for aerosol particle classification between 2 and 40 nm that can be interpreted as originally atmospheric particles with confidence (Asmi et al., 2009). The NAIS features two multichannel differential mobility analyzers, for detecting positively and negatively charged particles, respectively. By switching between different measurement modes, the NAIS can measure the mobility

distribution of particles after positive and negative charging ("particle mode") and also the mobility distribution of naturally charged particles and ions ("ion mode").

During our experiments two individual NAIS instruments were used. The instrument NAIS-4 was deployed at Melpitz between April 2008 and August 2009. Instrument NAIS-15 was deployed from June 2010 until October 2011. NAIS-4 was calibrated in January 2008, showing an average performance compared to four other NAIS instruments (Asmi et al., 2009). This performance could be verified in a follow-up calibration experiment in July 2009 (Gagné et al., 2011). At Melpitz, the NAIS instruments sampled ambient air through a dedicated stainless steel pipe (diameter: 3.5 cm, length: 160 cm) at a flow rate of 60 l min^{-1}. There were no obstacles in the NAIS sampling line except a metal grid that was designed to prevent insects from entering the instrument. The analyser columns of the instrument were cleaned every four weeks.

2.2.2 Twin DMPS and APS

Particle number size distributions were measured with a twin differential mobility particle size spectrometer (TDMPS). This instrument follows the principle design of Birmili et al. (1999), but circulates sheath air in a closed loop in compliance with recommendations for atmospheric aerosol particle number size distribution measurements (Wiedensohler et al., 2012). Briefly, the instrument consists of two differential mobility particle analyzers (Vienna type), connected to a condensation particle counter (model 3010, TSI, Shoreview (MN), USA), and an ultrafine condensation particle counter (model 3025, TSI), respectively, which encompass a total particle size range between 3 to 800 nm. A measurement cycle lasts for ten minutes.

Coarse particles were measured in an aerodynamic size range between 0.8 and 10 μm using an Aerodynamic Particle Sizer (model 3321, TSI). Both the TDMPS and the APS are connected to an automatic regenerating adsorption aerosol dryer (Tuch et al., 2009). This ensures relative humidities below 30 % at all times in the aerosol sample.

2.2.3 Merging multi-instrumental particle number size distributions

The NAIS, TDMPS and APS number size distributions were merged as follows: from 2–10 nm, NAIS data were employed exclusively. A reason is that the current Melpitz TDMPS set-up suffers from enhanced particle losses below 10 nm, because these measurements have been optimized with regard to long-term stability that involves the use of a regenerative dryer upstream of the instrument (see above). The extensive sampling system ensures low relative humidities in the sampling line at all times, but also causes non-recoverable particle losses at the lower tail of the TDMPS particle size distribution.

In the size range 10–20 nm, the NAIS and TDMPS number size distributions were cross-faded into each other using linear mixing as a function of logarithmic diameter between 10 nm (only NAIS) and 20 nm (only TDMPS). Above 20 nm, the NAIS size distributions become increasingly unreliable because the data inversion of that instrument does not take into account the multiple charges from particles bigger than 40 nm due to the limited size range of the instrument. Between 20 and 800 nm, TDMPS data were used exclusively, which exhibit their greatest reliability across this diameter range. Above 800 nm, APS data were used exclusively, after converting the aerodynamic into a mobility particle size distribution using an effective particle density of 1.7 g cm^{-3}.

2.2.4 Gas-phase measurements

Gaseous sulphuric acid (H_2SO_4) and the hydroxyl radical ($\cdot OH$) were measured at Melpitz during an intensive measurement period of EUCAARI (European integrated project on aerosol, cloud, climate, and air interactions) by Chemical Ionisation Mass Spectrometry (CIMS; Berresheim et al., 2002). These measurements lasted from 1 to 31 May 2008. To make an estimate of H_2SO_4 available for a longer period, we calculated a proximity measure, which was determined on the basis of this one-month data set (Sect. 2.3). Ammonia concentrations were measured by a Monitoring Instrument for AeRosols and GAses (MARGA, Metrohm Applikon B.V., Schiedam, the Netherlands).

Title Page

Abstract | Introduction

Conclusions | References

Tables | Figures

|◄ | ►|

◄ | ►

Back | Close

Full Screen / Esc

Printer-friendly Version

Interactive Discussion

2.2.5 Meteorological measurements

3d wind speed was sampled on a mast of 6 m height using a sonic anemometer (model USA-1, METEK GmbH, Elmshorn). The sampling frequency was 1 Hz. From the continuous time series, the turbulent heat flux $w'\theta'$ and the turbulent kinetic energy (TKE) were calculated for 15 min intervals.

2.3 Chemical mass balance model for sulphuric acid

Gaseous sulphuric acid (H_2SO_4) and hydroxyl radicals ($\cdot OH$) were only measured from 1–31 May 2008 (EUCAARI-2008). To scrutinize the relationship between H_2SO_4 and newly formed particles for the longer time period 2008–2011, the H_2SO_4 concentrations were estimated using a chemical mass balance model, driven by a solar radiation as a source of $\cdot OH$.

A proximity measure for $[H_2SO_4]$ at day-time conditions will need, in a first step, a proxy for $[\cdot OH]$. Rohrer et al. (2006) showed that there is a close relationship between $[\cdot OH]$ and the UV solar flux. The latter is closely correlated with global solar irradiance (Boy and Kulmala, 2001). Based on the experimental $[\cdot OH]$ from the EUCAARI-2008 campaign, we derived the following parameterization for Melpitz:

$$[\cdot OH] = A \cdot \mathrm{Rad}\,[\mathrm{cm}^{-3}] \tag{1}$$

where Rad is the global solar irradiance in $\mathrm{W\,m}^{-2}$ as measured by a pyranometer. The proportionality parameter A was derived by linear regression of these parameters for the EUCAARI-2008 data set, yielding a value of $6166\,\mathrm{m}^2\,\mathrm{W}^{-1}$ for A. See Fig. 1a for the corresponding scatter plot.

In a second step, H_2SO_4 concentrations were estimated using a modified version of the chemical mass balance model introduced by Weber et al. (1997):

$$[H_2SO_4] = B\frac{[\cdot OH][SO_2]}{\mathrm{CS}}\left[\mathrm{cm}^{-3}\right] \tag{2}$$

Evolution of gaseous precursors and meteorological parameters

J. Größ et al.

This mass balance assumes that OH radical attack on SO_2 is the process governing the production rate of H_2SO_4. Here, [·OH] is the hydroxyl radical concentration estimated from Eq. (1) in cm^{-3}, [SO_2] the measured sulphur dioxide concentration in cm^{-3}, B a constant related to the reaction rate of the two above mentioned species, and CS the condensation sink (Pirjola et al., 1999) in s^{-1} calculated for the particle number size distribution adjusted to ambient relative humidity. For this adjustment, an empirical growth law based on one year of hygroscopicity analyser measurements at Melpitz was used (see Appendix).

The term B[·OH][SO_2] represents the production term of H_2SO_4 and CS is the loss term of H_2SO_4 by condensation onto the pre-existing particle population. The parameter B was derived by regression analysis of measured and estimated [H_2SO_4] for 9 days of data during the EUCAARI-2008 campaign (Fig. 1b). Linear regression analysis yielded a value of 2.75×10^{-12} $cm^3 s^{-1}$ for B. It is worth to note that the parameter B seems to depend significantly on the observation site. Petäjä et al. (2009), for instance, obtained a value of 8.6×10^{-10} $cm^3 s^{-1}$ for the boreal forest site Hyytiälä, Finland.

For reasons of consistency, this H_2SO_4 parameterization was compared with the linear approximation formulae given by Mikkonen et al. (2011) (Table 3; formulaes L1–L5), which were previously applied for the same Melpitz data set. Mikkonen et al.'s formulae assume various linear and non-linear dependencies of [H_2SO_4] on Radiation, [SO_2], dry CS and relative humidity RH. Mikkonen et al. (2011) concluded that their formula (L3) was superior for the Melpitz EUCAARI-2008 data set. The correlations diagrams involving of all of Mikkonen's proximity measures with experimental [H_2SO_4] are shown in the Appendix, Fig. A1.

For this work, we ultimately preferred Eq. (2) for two reasons. First, it simulates CS from the particle size distribution (2 nm–10 µm) after adjustment to ambient relative humidity. (Mikkonen's proxies in Eq. (L0), (L1) and (L5) determined CS on the basis of a dry particle number size distribution). Second, Eq. (2) is based on a mass balance calculation, assumed to be valid at least for day-time conditions, and avoids some non-linear dependencies that lack a mechanistic explanation.

3 Exemplary NPF events

Fig. 2 introduces four cases of new particle formation (NPF) events at Melpitz covering a range of different observations. Contour diagrams show the particle number size distribution (2–1000 nm), the number concentration of freshly produced particles $N_{[2;20]}$
5 (aggregated from NAIS and TDMPS data), the condensational sink (CS), and the gas phase concentrations of SO_2, $\cdot OH$, and H_2SO_4. The four NPF events were chosen to represent a certain range of observations typical to NPF formation at Melpitz station, depending on environmental conditions and characteristic of NPF formation, based on our subjective judgement. The availability of solar radiation, as well as sunrise and
10 sunset can be followed by the calculated $\cdot OH$ concentration.

3.1 Case 1: NPF and subsequent growth under clean conditions (19 June 2010)

On 19 June 2010, the NPF and subsequent growth to ca. 50 nm was clearly visible (Fig. 2a). The NPF event started around 06:00 LT in a clean Atlantic air mass, as confirmed by back trajectories obtained from the HYSPLIT model. CS was constantly
15 low throughout the day, as was $[SO_2]$. Until 10:00 LT, the sky was cloudless, leading to $\cdot OH$ concentrations calculated from Eq. (1) around $4 \times 10^6\,cm^{-3}$. The combination of an ideal solar radiation flux, low CS and low $[SO_2]$ (1–$2 \times 10^{10}\,cm^{-3}$) yielded moderate calculated concentrations of H_2SO_4 around $2 \times 10^7\,cm^{-3}$. This case is an example where the production rate of H_2SO_4 depends on $[\cdot OH]$ more significantly than on $[SO_2]$.
20 In the event classification to follow in Sect. 4, this event was classified as a Class I particle formation event.

3.2 Case 2: NPF and subsequent growth under polluted conditions (29 May 2008)

Like above, the NPF event on 29 May 2008 was marked by a pronounced particle
25 growth up to around 60 nm (Fig. 2b). But in comparison to Case 1, significantly higher

levels of both, SO_2 and CS prevailed. Figure 2b reveals the trace of an Aitken mode (diameter around 60–100 nm) from the preceding day. The trace of this mode prevails even after NPF started around 09:00 LT. Back trajectory analysis confirmed the presence of continental air originating from easterly directions. The high H_2SO_4 production rate on this day derives primarily from the extraordinary high level of SO_2. The CS was nearly constant before and during the onset of NPF event and probably played minor role in the NPF formation and subsequent evolution of nanometer particles. In Sect. 4 this event is also classified as a Class I particle formation event.

3.3 Case 3: Short-lived stationary NPF event (7 June 2010)

This case represents a class of short-lived nucleation events, i.e. shorter than 2 h in duration (Fig. 2c). The NPF event started at 10:00 LT and was associated with a short peak in SO_2. The size range from 2 to 20 nm was uniformly filled with aerosol particles and no growth was observed. Solar radiation produced calculated [·OH] levels with maxima at around 5×10^6 cm^{-3} even later, but the cut-off of the NPF event was likely to be the decrease in [SO_2] from 12:00 LT. Back trajectory analysis suggested the advection of a clean maritime air mass from north westerly directions. CS showed moderate values around 0.01 s^{-1} during daytime, but elevated values up to about 0.05 s^{-1} during nighttime.

3.4 Case 4: Long-lived stationary NPF event (23 August 2008)

Like case 3, this event is characterized by the lack of particle growth (Fig. 2d). However, the duration of the NPF event was considerably longer than in Case 3, between 09:00 and 17:00 LT. Such observations can be thought to be the result of a continuous influence by a stationary source or process. On this day, rather clean air from westerly directions prevailed with CS below 0.005 s^{-1} after 05:00 LT like in Case 1. It might be worth to note that just before, CS decreased from a considerably higher night-time level of about 0.04 s^{-1} due to a change from continentally influenced towards maritime air.

We are not aware of any nearby source of SO_2 and/or particles which could explain the observation. Solar radiation and calculated [·OH] were fluctuating due to changes in cloudiness.

3.5 A comment on the patterns and shapes of NPF events

The case studies reveal that NPF events at Melpitz occur in a great variety of patterns and shapes. One essential reason for this variety is the stationary nature of the point measurements. During the measurement, air masses of more or less diverging composition blow past the measurement site. Melpitz is located in Central Europe, a region, where spatial gradients in air composition are a regular feature. Only if the wind speed is low compared to these gradients, an idealistic observation of new particle formation and growth, i.e. involving smooth changes and continuous observations can be expected. Besides air mass changes due to advection, the atmosphere almost always involves vertical mixing during the periods of NPF events, due to convection aroused by intense solar radiation. If air aloft contains different concentrations of trace gases and/or aerosol particles, concentrations near the ground will inevitably change even during the NPF process. To some surprise, these issues only play a marginal role in the wide body of literature on experimental NPF studies. It therefore represents a great challenge to examine and quantify the ongoing processes simply on the basis of ground-based measurements. While efforts have been made to characterise the atmosphere during NPF events vertically and spatially (Stratmann et al., 2003) such observations will only yield a limited number of observations, and usually a restricted set of parameters that can technically be measured on an airborne platform. To examine the statistical relevance of the NPF process, long-term data sets are needed, which inevitably require some categorisation or classification. The next chapter is therefore dedicated to the classification of NPF events at Melpitz, making use of the extended set of aerosol parameters available.

4   NPF event classification

To examine gas phase precursor and meteorological effects as a function of new particle formation (NPF) intensity, we conceived a new method to classify the set of measured NPF events. The method is based on a convolution integral (CI) of time series of the number concentration of freshly nucleated particles ($N_{[2;20]}$). The convolution integral is defined by:

$$\mathrm{CI}(\tau) = (f \ast g)(\tau) = \int f(t)\, g(\tau - t)\, \mathrm{d}t \tag{3}$$

where $f(t)$ is the time series of $N_{[2;20]}$, as averaged from a number of 27 manually selected NPF events and $g(\tau)$ the measured time series of $N_{[2;20]}$. τ is a time lag. The 27 selected NPF events featured very high peak values of $N_{[2;20]}$ and subsequent particle growth up to maximum diameters of 100 nm on the same day. (The two events in Fig. 2a and b are typical representatives of this selection.) $f(t)$ was calculated as an average of these time series of $N_{[2;20]}$, however, with the time series centred around their peak value. In time, $f(t)$ contains experimental values from 5 h prior to the maximum in $N_{[2;20]}$ to 10 h after. Outside this interval, $f(t)$ was set to zero. No normalisation was made to the amplitude of $N_{[2;20]}$. In simple words, f represents an idealistic temporal evolution of $N_{[2;20]}$ during the most intense NPF events. A complete list of the 27 NPF with their associated maximum concentrations of $N_{[2;20]}$ is supplied in Table A1 in the Appendix.

In a second step, the time series of the CI was analysed for peak values. CI reaches a peak at the times when the peaks of f and g coincide. Because CI is calculated as an integral over concentration and time, higher peak values are reached when the NPF event represented by g extends in time (cf. Fig. 2a and b) rather than being a short-lived event (cf. Fig. 2c). This means that CI is not only sensitive to the absolute peak values of $N_{[2;20]}$ but also to the duration of the NPF event. Figure 3a illustrates a sample of the time series of CI with maximum values attained during mid-day, i.e. when NPF events take place.

In a third step, the peaks in CI(t) were detected, and their peak values CI_{peak} subsequently classified according to their magnitude. Only the NPF events with peaks in CI occurring between sunrise and sunset were taken into account, i.e. those that can apparently be related to photochemical processes. (In fact, no significant nucleation was observed in Melpitz outside this period anyway.) Fig. 3b presents all peaks identified between sunrise and sunset as a function of time of day. As discussed before, the peak height is a combined measure of the attained particle number concentration $N_{[2;20]}$ and the event duration. From the data cloud in Fig. 3b, three event classes were defined as follows: Class I, showing CI_{peak} in the range 3×10^8–$1.2 \times 10^9\,s\,cm^{-6}$, Class II with CI_{peak} in the range 7×10^7–$3 \times 10^8\,s\,cm^{-6}$, and Class III with CI_{peak} below $7 \times 10^7\,s\,cm^{-6}$ (see Table 2).

The motivation of the boundaries between the event classes is as follows: Class III represents the 83 NPF events of lowest intensity. As the NAIS instrument is very sensitive, it is able to detect short-lived peaks of small particles, even at very low concentration. In fact, a peak of $N_{[2;20]}$ can be defined for each day, no matter how low it might be. As can be seen from Fig. 3b, these short and low peaks may take place any time between sunrise and sunset. We associate these very weak events with very small-scale particle bursts that do not evolve into a fully developed and spatially distributed nucleation event. In any case, this class of observations includes what most researchers would call "non-events".

Class II represents 92 NPF events that take place at least a few hours after sunrise, i.e. when the atmospheric boundary layer has started to mix vertically. These events are usually longer-lived, and reach higher concentrations in $N_{[2;20]}$. The requirement of Class II events to surpass the threshold $CI_{peak} = 7 \times 10^7\,s\,cm^{-6}$ is clearly motivated from the shape of the data cloud in Fig. 3b: below this threshold, short incidents of small particles may take place any time between 05:00 and 18:00, while the events above this threshold always exhibit a start time between sunrise and sunset.

Class I, in turn, represents the 94 most intense NPF events. These are always associated with high absolute values of $N_{[2;20]}$ and an event duration over several hours.

Most of them, although not all, showed the clear particle growth pattern visible in Figs. 2a and b. The threshold in CI_{peak} between Class I and Class II events is somewhat arbitrary. In fact, we are facing a continuum of observations ranging from the lowest to the highest observations in NPF intensity. Guided by practical needs, we have attempted to create data sub-sets of similar dimension, and have also tried to define a threshold above which the obvious particle growth pattern is a clear majority. This led to the threshold value of $2 \times 10^8 \, s \, cm^{-6}$.

The introduction of a new NPF classification method requires some justification. Continuous observations of NPF events in the continental boundary layer with particle mobility spectrometers in the mid-1990s. (Continuous monitoring of air ions dates back even further, until the 1980s; Hõrrak et al., 2003, and references therein). Since then, there have been various attempts to classify NPF events according to their relevant features and parameters including the following approaches:

1. The University of Helsinki classification (Dal Maso et al., 2005): this elaborate method has been widely used to classify NPF events after several criteria, including the existence of a continuous trace of a nucleation mode starting in the nucleation mode range, and whether apparent particle formation and growth rates can be calculated with confidence. Somewhat problematic is the softness of some criteria, such as whether the "mode concentration and diameter fluctuate strongly". Recent work has refined the mode classification (Buenrostro Mazon et al., 2009; Manninen et al., 2010; Hirsikko et al., 2011), now classifying many previously "undefined" new particle formation events.

2. Methods based on peak values in absolute particle number concentration, sometimes requiring a certain shape of the time evolution of the time series of nucleation mode particle number concentration (e.g., Birmili et al., 2003).

3. Identification of new particle formation events based on the similarity of the time series of multiple particle number size distribution moments (Heintzenberg et al., 2007).

Our newly developed scheme is tailored to the combined NAIS-TDMPS observations at the rural background Melpitz for the following reasons:

- The number of freshly formed particles (here $N_{[2;20]}$) is, after all, the most basic and most important indicator of recent particle nucleation. Any other parameters, such as apparent particle formation rates (often estimated by $\Delta N / \Delta t$, or by a time delay between precursor concentrations and N) or particle growth rates, are subject to inherent uncertainties, such as those induced through air mass changes by convection and/or advection (cf. Sect. 3.5).

- At Melpitz, we found it hard to quantify the particle growth of neutral particles in the nucleation mode below 10 nm by tracking the mode in the NAIS size distributions. The observations tell that if particles appear in significant numbers at the surface-based research station, they will appear across the entire interval 2–10 nm, or even beyond (cf. Fig. 2a–d). When the total particle number concentration reaches its maximum, the size distribution of the nucleation mode particles has very often reached the region of 20 nm already (Fig. 2a–d). Above that range 10–20 nm, the subsequent particle growth can usually be followed nicely using the TDMPS-based range of the size distribution (Fig. 2a and b). These observations, however, are the justification to use $N_{[2;20]}$ as the best indicator for a NPF event. The relatively wide interval $N_{[2;20]}$ has also a technical advantage that it produces a statistically sound signal with a low noise level.

- Our method avoids the common problem of rigorously distinguishing between NPF events and non-events. Acknowledging the true observable continuum of observations between "zero" and top level concentrations, we rather introduce three classes according to different degrees of NPF intensity.

- Our method has a high degree of objectivity. (This means that it can be written down in a way that any other researcher can reach exactly the same classification results). This makes it similar to the approach by Heintzenberg et al. (2007).

Some subjectivity arises from the choice of the 27 NPF events that serve as a "calibration" of the method (Table A1), and from the threshold values for CI_{peak} selected to separate the events into Classes I, II and III, although these criteria can be written down explicitly (Table 2).

The comparison between the CI method and the University of Helsinki classification (Dal Maso et al., 2005) is shown in Table A2. Naturally, the two methods show a strong correlation when distinguishing between different degrees of observed particle formation. UHEL class 1a, coincides, for example to 72 % with CI Class I. UHEL non-events coincide to 85 % with the analogous CI class 3. On the other hand, CI Class I splits up more evenly into UHEL classes 1a, 1b and 2. One reason is that the UHEL scheme evaluates additional formal issues, such as whether a NPF event shows a clear trace in the nucleation mode (i.e unobstructed by background aerosol) or not. These are not issues in the CI method, which weighs primarily the number concentration of the observed particles and the duration of a NPF event.

5   Correlations with gas phase and meteorological parameters

5.1   Time evolution of NPF events

Having classified NPF events into strong, medium and weak NPF events, we now scrutinize the entire data set for correlations with gaseous precursors and meteorological parameters. Figure 4 shows average diurnal cycles of measured atmospheric parameters that are considered relevant for the NPF process. Importantly, all diurnal cycles were moved in time prior to averaging so that their peak in CI coincides with $t = 0$. Each curve represents an arithmetic average over all days within the subsets defined in Table 3. [·OH] and [H_2SO_4] were estimated by the proximity measures in Eq. (1) and (2). The ternary nucleation rates TNR were calculated according to Napari et al. (2002) using the in-situ measurements or estimates for T, RH, [H_2SO_4] and [NH_3]. Because of the limited data availability of [NH_3] (2010 and 2011), a sensitivity analysis for ammonia

concentrations was performed separately (see Fig. A3). Since the inclusion of ammonia in the analysis did not alter our conclusions, we feel confident in basing the conclusions on the full observation period 2008–2011, and the constraint of using a constant ammonia concentration of 5 ppt.

5 **Time around sunrise (−6 h)**

We start the description 6 h prior to the event peak time, which is ca. 04:40 LT for Class I events, ca. 05:50 LT for Class II events, and ca. 05:10 for Class III events. This is the time before, or just around sunrise on most of these days.

10 At this time, we see no or only very little indication from the locally measured parameters whether a NPF will happen or not a few hours later, and which intensity the event will have: solar radiation and $[\cdot OH]_{calc}$ are low, around 0.7–1.2×10^6 cm^{-3}. Ozone levels are very similar for all event classes, around 6×10^{11} g m^{-3}. $[SO_2]$ is the same for all event classes, just below 1.1×10^{10} cm^{-3}, as is RH at around 88 % on arithmetic average. $[H_2SO_4]_{calc}$ is at negligible levels, as is ternary nucleation rate (TNR). 15 (As mentioned above, TNR was calculated according to Napari et al., 2002). Also, the turbulent heat flux available for the 2010 measurements ($w'\theta'$) is very similar around 0.01–0.025 K m s^{-1}.

The few minor indications for NPF events to come are: (1) Class I events show early morning temperatures below average. (2) Class I and II events show turbulent kinetic 20 energy (TKE; cf. Sect. 2.2.5) below average. (3) Class I and II events show a condensation sink CS above average. The meteorological indications (1) and (2) point to a surface layer that is highly stratified and calm in the morning of NPF events. As will be explained later, the increased CS is a conspicuous indicator that semi-volatile compounds have accumulated in the particle phase.

Title Page

Abstract | Introduction

Conclusions | References

Tables | Figures

|◀ | ▶|

◀ | ▶

Back | Close

Full Screen / Esc

Printer-friendly Version

Interactive Discussion

First indications of NPF event (−3 h)

Three hours before event peak time, the evolution of many parameters are already indicative of a NPF event to happen or not. Most important, solar radiation ($[\cdot OH]_{calc}$) is substantially higher on Class I and II event days compared to Class III event days. As a direct response, the near-surface temperature T is rising rapidly, and RH is decreasing. CS is rapidly decreasing on the Class I and II days, which is assumed to be due partly to the repartitioning of semi-volatile compounds (ammonium nitrate as well as semi-volatile organic matter) from the particulate into the gas phase. Evidence for the relevance of the latter process at Melpitz was given by aerosol mass spectrometric measurements on days with high solar radiation (Poulain et al., 2011). Three hours before event peak time, a significant increase in absolute humidity can be seen on Class I and II days. This is interpreted as the vaporisation of the dew covering the grassland surrounding the Melpitz site.

A key observation is the increase in $[SO_2]$ on Class I and II event days around 3 h before event peak time. From this time, the number of newly formed particles $N_{[2;20]}$ increases in proportion with $[SO_2]$. It needs to be noted that within a radius of 100 km around Melpitz, sources of SO_2 are scarce. In Germany, SO_2 is emitted in noticeable quantities by single point sources (power plants), and domestic heating. Point sources are, as a matter of fact, far away from Melpitz while domestic heating is likely to be irrelevant in the warm season of concern. Our interpretation is that the morning increase in near-surface $[SO_2]$ is caused by a combination of two processes: (i) First, $[SO_2]$ depletes at night due to dry deposition onto the surface. Deposition of SO_2 onto the surface was confirmed in early experiments at Melpitz by gradient measurements (Spindler et al., 1996). This depletion of near-surface $[SO_2]$ yields the typical values of 1.1×10^{10} cm^{-3} in the early morning hours, regardless whether a NPF event will take place of not (cf. Fig. 4b). (ii) Vertical mixing, starting gradually after sunrise, will cause entrainment of SO_2 from greater heights where SO_2 did not have the opportunity to deposit. During past field experiments in Melpitz, nocturnal low-level jets have shown

to advect SO_2 at greater heights, which were entrained to the ground after the onset of convection (Beyrich, 1994). (Nocturnal low level jets originate from geostrophic winds, and are able to advect air over long distances above a firm temperature inversion near the ground.) In this experiment we did not have the means to verify their relevance.

Maximum in nucleation mode number concentration (0 h)

Event peak time ($t = 0$) was defined by the maximum in freshly formed particles $N_{[2;20]}$. Class I events feature arithmetic mean concentrations around $1.1 \times 10^5\,cm^{-3}$, Class II events around $3.7 \times 10^4\,cm^{-3}$ (Fig. 4a). Event peak time coincides with the maximum of solar radiation and $[\cdot OH]_{calc}$ (Fig. 4c). $[SO_2]$, $[H_2SO_4]_{calc}$ and TNR scale in proportion to the event class. It is worth to note that on Class I days $[SO_2]$ exhibits an additional steep rise just before event peak time, emphasizing the strong connection between $N_{[2;20]}$ and $[SO_2]$. This peak translates into the proxy $[H_2SO_4]_{calc}$ and TNR as well. T, RH, and $[O_3]$ do not significantly differ between Class I and II events at $t = 0$; they show the typical features of a near-surface measurement on a cloudless day. Absolute humidity decreases on Class I and II towards the middle of the day, which is interpreted as mixing with relatively dry air from aloft. It is noteworthy that on Class I event days, CS increases just in time with the maximum of $N_{[2;20]}$, and along with a continuing rise in $[SO_2]$. In several case studies, we observed something which we interpreted as the simultaneous entrainment of SO_2 and CS (e.g., 2008-08-23 in Fig. 2). CS is correlated with the number of bigger particles, in the Aitken and accumulation mode. It is our interpretation that in these cases, CS originates from the same or similar pollution sources that emit SO_2. (The newly formed particles $< 20\,nm$ themselves are, in fact, too small to significantly contribute to CS.)

Development after event peak time ($t > 0$ h)

After event peak time, the parameters $N_{[2;20]}$, $[\cdot OH]_{calc}$, $[H_2SO_4]_{calc}$ and TNR decrease to their mean levels within a matter of a few hours. It is an interesting feature that for

both, Class I and II events the peak in [SO$_2$], like the peaks in [H$_2$SO$_4$]$_{calc}$ and TNR, occurs around one hour later than the peak in $N_{[2;20]}$. This implies that the entrainment of air rich in [SO$_2$] continues even after some other parameter has started to waive the nucleation process.

5.2 Micrometeorological parameters

For the third measurement period in 2010, 3d wind was measured at one second resolution 6 m above the ground with an ultrasonic anemometer. From the 3d wind velocities, various turbulence parameters were calculated with a time resolution of 15 min. In Fig. 5 we illustrate those parameters that proved most sensitive to the class of NPF event, the turbulent heat flux $w'\theta'$ and the turbulent kinetic energy (TKE). The actual number of days for which these data were available is listed in Table 6.

A prime result is that in all cases of Class I and II events, the boundary layer was turbulently mixed. In fact, we could not see a significant difference between Class I and II days with respect to the turbulence parameters. In contrast, a rather weak flux and TKE prevailed on Class III events. The diurnal evolution of the turbulence parameters is in close correspondence with the development of solar radiation and temperature (Fig. 4).

5.3 Statistical significance

We performed statistical tests in order to identify significant differences between the three NPF event categories in terms of the measured atmospheric parameters. Student t tests were conducted at a significance level of 99 % for every 15 min intervals for the parameters shown in Fig. 4.

5.4 Examining the particle formation rate J_2

To round up the discussion of process parameters derived from the NPF events, formation rates of 2 nm particles (J_2) were determined from the particle number size dis-

Title Page

Abstract | Introduction

Conclusions | References

Tables | Figures

|◀ | ▶|

◀ | ▶

Back | Close

Full Screen / Esc

Printer-friendly Version

Interactive Discussion

tributions measured by NAIS. The number concentration of particles in the size range 2–3 nm, N_{2-3}, was integrated from the measured size distributions. The formation rate J_2 was calculated from the time derivative of N_{2-3}, taking into account the coagulation losses of 2–3 nm particles into larger particles and condensation growth out of the 2–3 nm size range as described in Kulmala et al. (2012).

Figure A4 shows the correlation between the calculated ternary nucleation rate TNR, and the measured number concentration N_{2-20} of 2–20 nm particles with the calculated H_2SO_4 concentration. Figure A5 shows corresponding data for the particle formation rate J_2. Interestingly, N_{2-20} seems to correlate more strongly with H_2SO_4 than J_2 or TNR. One reason for the lower correlation between J_2 and H_2SO_4 could be that the calculated J_2 values can be more uncertain the directly measured N_{2-20} concentrations, making the J_2 vs. H_2SO_4 more scattered. The J_2 values obtained in this study fall within the same correlation with H_2SO_4 as observations made at other sites during the EUCAARI 2008–2009 campaign (right graph in Fig. A5; reproduced from Kerminen et al., 2010).

5.5 Discussion

As can be seen in Fig. 4, the intensity of newly formed particles (expressed by the three different classes based on $N_{[2;20]}$) correlates with $[\cdot OH]_{calc}$, $[H_2SO_4]_{calc}$, $[SO_2]$, and TNR on a diurnal scale. The most significant discrepancy between Class I/II and Class III events is made up by different levels of global radiation, manifested by $[\cdot OH]_{calc}$. It can also be seen that peaks in $N_{[2;20]}$ and $[\cdot OH]_{calc}$ coincide within 30 min for event Class I and II. This simple and rather established correlation between nucleation mode particles and solar radiation (e.g., Boy and Kulmala, 2001) seems to represent the most basic impact influencing NPF at Melpitz.

$[H_2SO_4]_{calc}$ turns out to be another major influential factor as well: the magnitudes of the daily peaks in $N_{[2;20]}$ and $[H_2SO_4]_{calc}$ scale in proportion across the three different classes. The effect of $[H_2SO_4]_{calc}$ can be broken down into the effects of $[SO_2]$, $[\cdot OH]_{calc}$ and CS. The difference in $[H_2SO_4]_{calc}$ between Classes I/II and III is mainly made up

by radiation ($[\cdot OH]_{calc}$) while the difference in $[H_2SO_4]_{calc}$ between Classes I and II is accounted for by different levels of $[SO_2]$ primarily. The effect caused by differences in CS is comparatively minor; CS is slightly lower during Class II events than during Class III events, allowing for a higher steady-state $[H_2SO_4]_{calc}$. The combination of the in-situ measurements or estimates for T, RH, $[H_2SO_4]$ also yield the ternary particle nucleation rate shown in Fig. 4i. This essentially propagates the trend found for $[H_2SO_4]_{calc}$, but does not yield significant new insights.

We obtained the following descriptions of different classes of NPF events at Melpitz:

  – Class I: Days with significant solar radiation, and high $[SO_2]$ levels

  – Class II: Days with significant solar radiation, but average $[SO_2]$ levels

  – Class III (containing weak events and non-events): days with significant cloud cover

Many other features, such as the trend towards high temperatures (T), low relative humidities (RH), and a higher ozone mixing ratio $[O_3]$ can be directly linked to solar radiation as the prime source of these meteorological and photochemical processes. It is intriguing that the diurnal cycles of T, RH, $[O_3]$, and $[\cdot OH]_{calc}$, $w'\theta'$ and TKE are very similar for the event classes I and II, but rather different from those in event Class III (including non-events). This suggests that the meteorological and photochemical processes on the days of Class I and II events are very similar.

6   Conclusions

This paper revisited the new particle formation process (NPF) in the Central European boundary layer at the Melpitz station, using a new data set involving neutral cluster and air ion spectrometer (NAIS) data for 2008–2011. Particle formation events were classified by an automated method based on the convolution integral of particle number concentration in the diameter range 2–20 nm. In analogy to previous field studies,

the intensity of solar radiation was confirmed as the main factor controlling the occurrence of NPF events. The absolute number of observed particles in the diameter range 2–20 nm, however, varied mainly in proportion with the concentration of sulfur dioxide as the presumed main precursor of sulfuric acid. This is consistent with a model picture that UV radiation is instrumental in generating OH radicals which, in turn, form H_2SO_4 via OH radical attack on SO_2. The condensational sink CS as a factor potentially inhibiting NPF events apparently played a subordinate role only. The same held for experimentally determined ammonia concentrations, a potential precursor of particle nucleation. It thus appears that at Melpitz, ammonia seems to be available always in excess.

The analysis of micrometeorological turbulence parameters demonstrated the presence of significant turbulence in the boundary layer on NPF events. Due to its close correlation with solar radiation, however, an independent effect of turbulence for NPF could not be established with certainty. An analysis of the diurnal cycles of aerosol, gas phase, and meteorological parameters suggest that particle nucleation tends to happen some way aloft in the residual layer. The according arguments are the night-time depletion of sulfur dioxide near the surface, the higher probability of particle nucleation at lower temperatures aloft, as well as the frequent observation of larger scale particles, e.g. 10–20 nm diameter, at the on-set of observed nucleation at the ground.

Appendix A

For the adjustment of particle number size distribution to ambient relative humidity (Sect. 2.3), an empirical growth law based on an entire year (II/2008-I/2009) of hygroscopicity analyzer (H-TDMA) measurements at Melpitz was used. The growth factors were measured at 90 % RH for the dry particle diameters 50, 75, 110, 165, and 265 nm. Parts of those data are illustrated in Zieger et al. (2014). The formula allows to compute the hygroscopic growth factor as a function of dry particle diameter and relative

humidity as follows:

$$\text{HGF}\left(D_{\text{p}}, \text{RH}\right) = \left(1 - \frac{\text{RH}}{100}\right)^{\gamma(D_{\text{p}})\frac{\text{RH}}{100}}, \gamma\left(D_{\text{p}}\right) = 0.20227 - \frac{0.1082}{1 + e^{\frac{D_{\text{p}} - 118.4}{21.35}}} \tag{A1}$$

References

Almeida, J., Schobesberger, S., Kürten, A., Ortega, I. K., Kupiainen-Määttä, O., Praplan, A. P., Adamov, A., Amorim, A., Bianchi, F., Breitenlechner, M., David, A., Dommen, J., Donahue, N. M., Downard, A., Dunne, E., Duplissy, J., Ehrhart, S., Flagan, R. C., Franchin, A., Guida, R., Hakala, J., Hansel, A., Heinritzi, M., Henschel, H., Jokinen, T., Junninen, H., Kajos, M., Kangasluoma, J., Keskinen, H., Kupc, A., Kurtén, T., Kvashin, A. N., Laaksonen, A., Lehtipalo, K., Leiminger, M., Leppä, J., Loukonen, V., Makhmutov, V., Mathot, S., McGrath, M. J., Nieminen, T., Olenius, T., Onnela, A., Petäjä, T., Riccobono, F., Riipinen, I., Rissanen, M., Rondo, L., Ruuskanen, T., Santos, F. D., Sarnela, N., Schallhart, S., Schnitzhofer, R., Seinfeld, J. H., Simon, M., Sipilä, M., Stozhkov, Y., Stratmann, F., Tomé, A., Tröstl, J., Tsagkogeorgas, G., Vaattovaara, P., Viisanen, Y., Virtanen, A., Vrtala, A., Wagner, P. E., Weingartner, E., Wex, H., Williamson, C., Wimmer, D., Ye, P., Yli-Juuti, T., Carslaw, K. S., Kulmala, M., Curtius, J., Baltensperger, U., Worsnop, D. R., Vehkamäki, H., and Kirkby, J.: Molecular understanding of sulphuric acid–amine particle nucleation in the atmosphere, Nature, 502, 359–363, doi:10.1038/nature12663, 2013.
Asmi, A., Wiedensohler, A., Laj, P., Fjaeraa, A.-M., Sellegri, K., Birmili, W., Weingartner, E., Baltensperger, U., Zdimal, V., Zikova, N., Putaud, J.-P., Marinoni, A., Tunved, P., Hansson, H.-C., Fiebig, M., Kivekäs, N., Lihavainen, H., Asmi, E., Ulevicius, V., Aalto, P. P., Swietlicki, E., Kristensson, A., Mihalopoulos, N., Kalivitis, N., Kalapov, I., Kiss, G., de Leeuw, G., Henzing, B.,

Harrison, R. M., Beddows, D., O'Dowd, C., Jennings, S. G., Flentje, H., Weinhold, K., Meinhardt, F., Ries, L., and Kulmala, M.: Number size distributions and seasonality of submicron particles in Europe 2008–2009, Atmos. Chem. Phys., 11, 5505–5538, doi:10.5194/acp-11-5505-2011, 2011.

Asmi, E., Sipilä, M., Manninen, H. E., Vanhanen, J., Lehtipalo, K., Gagné, S., Neitola, K., Mirme, A., Mirme, S., Tamm, E., Uin, J., Komsaare, K., Attoui, M., and Kulmala, M.: Results of the first air ion spectrometer calibration and intercomparison workshop, Atmos. Chem. Phys., 9, 141–154, doi:10.5194/acp-9-141-2009, 2009.

Berresheim, H., Elste, T., Plass-Dülmer, C., Eisele, F. L., and Tanner, D. J.: Chemical ionization mass spectrometer for long-term measurements of atmospheric OH and H_2SO_4, Int. J. Mass Spectrom., 202, 91–109, 2002.

Beyrich, F.: Determination of mixed layer heights from SODAR data using numerical model calculations (translated from German), PhD thesis, Freie Universität Berlin, Berlin, 1994.

Birmili, W. and Wiedensohler, A.: New particle formation in the continental boundary layer: meteorological and gas phase parameter infiuence, Geophys. Res. Lett., 27, 3325–3328, 2000.

Birmili, W., Stratmann, F., and Wiedensohler, A.: Design of a DMA-based size spectrometer for a large particle size range and stable operation, J. Aerosol Sci., 30, 549–553, 1999.

Birmili, W., Wiedensohler, A., Heintzenberg, J., and Lehmann, K.: Atmospheric particle number size distribution in Central Europe: statistical relations to air masses and meteorology. J. Geophys. Res. D23, 32005–32018, 2001.

Birmili, W., Berresheim, H., Plass-Dülmer, C., Elste, T., Gilge, S., Wiedensohler, A., and Uhrner, U.: The Hohenpeissenberg aerosol formation experiment (HAFEX): a long-term study including size-resolved aerosol, H_2SO_4, OH, and monoterpenes measurements, Atmos. Chem. Phys., 3, 361–376, doi:10.5194/acp-3-361-2003, 2003.

Birmili, W., Weinhold, K., Nordmann, S., Wiedensohler, A., Spindler, G., Müller, K., Herrmann, H., Gnauk, T., Pitz, M., Cyrys, J., Flentje, H., Nickel, C., Kuhlbusch, T. A. J., Löschau, G., Haase, D., Meinhardt, F., Schwerin, A., Ries, L., and Wirtz, K.: Atmospheric aerosol measurements in the German Ultrafine Aerosol Network (GUAN) – Part 1: soot and particle number size distributions, Gefahrst. Reinh. Luft, 69, 137–145, 2009.

Boy, M. and Kulmala, M.: Nucleation events in the continental boundary layer: Influence of physical and meteorological parameters, Atmos. Chem. Phys., 2, 1–16, doi:10.5194/acp-2-1-2002, 2002.

Title Page

Abstract | Introduction

Conclusions | References

Tables | Figures

◀ | ▶

◀ | ▶

Back | Close

Full Screen / Esc

Printer-friendly Version

Interactive Discussion

Buenrostro Mazon, S., Riipinen, I., Schultz, D. M., Valtanen, M., Dal Maso, M., Sogacheva, L., Junninen, H., Nieminen, T., Kerminen, V.-M., and Kulmala, M.: Classifying previously undefined days from eleven years of aerosol-particle-size distribution data from the SMEAR II station, Hyytiälä, Finland, Atmos. Chem. Phys., 9, 667–676, doi:10.5194/acp-9-667-2009, 2009.

Dal Maso, M., Kulmala, M., Riipinen, I., Wagner, R., Hussein, T., Aalto, P. P., and Lehtinen, K. E. J.: Formation and growth of fresh atmospheric aerosols: eight years of aerosol size distribution data from SMEAR II, Hyytiälä, Finland, Boreal Env. Res., 10, 323–336, 2005.

Easter, R. C. and Peters, L. K.: Binary homogeneous nucleation: temperature and relative humidity fluctuations, nonlinearity, and aspects of new particle production in the atmosphere, J. Appl. Meteorol., 33, 775–784, 1994.

Engler, C., Rose, D., Wehner, B., Wiedensohler, A., Brüggemann, E., Gnauk, T., Spindler, G., Tuch, T., and Birmili, W.: Size distributions of non-volatile particle residuals ($D_p < 800$ nm) at a rural site in Germany and relation to air mass origin, Atmos. Chem. Phys., 7, 5785–5802, doi:10.5194/acp-7-5785-2007, 2007.

Fuchs, N. A. and Sutugin, A. G.: Highly dispersed aerosols, in: Vol H of Topics in Current Aerosol Research, Pergamon Press, New York, 1971.

Gagné, S., Lehtipalo, K., Manninen, H. E., Nieminen, T., Schobesberger, S., Franchin, A., Yli-Juuti, T., Boulon, J., Sonntag, A., Mirme, S., Mirme, A., Hõrrak, U., Petäjä, T., Asmi, E., and Kulmala, M.: Intercomparison of air ion spectrometers: an evaluation of results in varying conditions, Atmos. Meas. Tech., 4, 805–822, doi:10.5194/amt-4-805-2011, 2011.

Hamed, A., Birmili, W., Joutsensaari, J., Mikkonen, S., Asmi, A., Wehner, B., Spindler, G., Jaatinen, A., Wiedensohler, A., Korhonen, H., Lehtinen, K. E. J., and Laaksonen, A.: Changes in the production rate of secondary aerosol particles in Central Europe in view of decreasing SO_2 emissions between 1996 and 2006, Atmos. Chem. Phys., 10, 1071–1091, doi:10.5194/acp-10-1071-2010, 2010.

Haywood, J. and Boucher, O.: Estimates of the direct and indirect radiative forcing due to tropospheric aerosols: a review, Rev. Geophys., 38, 513–543, 2000.

Heintzenberg, J., Wehner, B., and Birmili, W.: "How to find bananas in the atmospheric aerosol": new approach for analyzing atmospheric nucleation and growth events, Tellus B, 59, 273–282, 2007.

Hirsikko, A., Nieminen, T., Gagné, S., Lehtipalo, K., Manninen, H. E., Ehn, M., Hõrrak, U., Kerminen, V.-M., Laakso, L., McMurry, P. H., Mirme, A., Mirme, S., Petäjä, T., Tammet, H.,

Title Page

Abstract | Introduction

Conclusions | References

Tables | Figures

|◀ | ▶|

◀ | ▶

Back | Close

Full Screen / Esc

Printer-friendly Version

Interactive Discussion

Vakkari, V., Vana, M., and Kulmala, M.: Atmospheric ions and nucleation: a review of observations, Atmos. Chem. Phys., 11, 767–798, doi:10.5194/acp-11-767-2011, 2011.

Hõrrak, U., Salm, J., and Tammet, H.: Diurnal variation in the concentration of air ions of different mobility classes in a rural area, J. Geophys. Res., 108, 4653, doi:10.1029/2002JD003240, 2003.

IPCC: Climate Change 2013: The Physical Science Basis, Contribution of Working Group I to the Fifth Assessment Report of the Intergovernmental Panel on Climate Change, edited by: Stocker, T. F., Qin, D., Plattner, G.-K., Tignor, M., Allen, S. K., Boschung, J., Nauels, A., Xia, Y., Bex, V., and Midgley, P. M., Cambridge University Press, Cambridge, UK and New York, NY, USA, 1535 pp, 2013.

Jeong, C.-H., Evans, G. J., McGuire, M. L., Chang, R. Y.-W., Abbatt, J. P. D., Zeromskiene, K., Mozurkewich, M., Li, S.-M., and Leaitch, W. R.: Particle formation and growth at five rural and urban sites, Atmos. Chem. Phys., 10, 7979–7995, doi:10.5194/acp-10-7979-2010, 2010.

Kerminen, V.-M., and Kulmala, M.: Analytical formulae connecting the "real" and the "apparent" nucleation rate and the nuclei number concentration for atmospheric nucleation events, J. Aerosol Sci., 33, 609–622, 2002.

Kerminen, V.-M., Petäjä, T., Manninen, H. E., Paasonen, P., Nieminen, T., Sipilä, M., Junninen, H., Ehn, M., Gagné, S., Laakso, L., Riipinen, I., Vehkamäki, H., Kurten, T., Ortega, I. K., Dal Maso, M., Brus, D., Hyvärinen, A., Lihavainen, H., Leppä, J., Lehtinen, K. E. J., Mirme, A., Mirme, S., Hõrrak, U., Berndt, T., Stratmann, F., Birmili, W., Wiedensohler, A., Metzger, A., Dommen, J., Baltensperger, U., Kiendler-Scharr, A., Mentel, T. F., Wildt, J., Winkler, P. M., Wagner, P. E., Petzold, A., Minikin, A., Plass-Dülmer, C., Pöschl, U., Laaksonen, A., and Kulmala, M.: Atmospheric nucleation: highlights of the EUCAARI project and future directions, Atmos. Chem. Phys., 10, 10829–10848, doi:10.5194/acp-10-10829-2010, 2010.

Kerminen, V.-M., Paramonov, M., Anttila, T., Riipinen, I., Fountoukis, C., Korhonen, H., Asmi, E., Laakso, L., Lihavainen, H., Swietlicki, E., Svenningsson, B., Asmi, A., Pandis, S. N., Kulmala, M., and Petäjä, T.: Cloud condensation nuclei production associated with atmospheric nucleation: a synthesis based on existing literature and new results, Atmos. Chem. Phys., 12, 12037–12059, doi:10.5194/acp-12-12037-2012, 2012.

Kulmala, M., Vehkamäki, H., Petäjä, T., Dal Maso, M., Lauri, A., Kerminen, V.-M., Birmili, W., and McMurry, P. H.: Formation and growth of ultrafine atmospheric particles: a review of observations, J. Aerosol Sci., 35, 143–176, 2004.

Kulmala, M., Asmi, A., Lappalainen, H. K., Baltensperger, U., Brenguier, J.-L., Facchini, M. C., Hansson, H.-C., Hov, Ø., O'Dowd, C. D., Pöschl, U., Wiedensohler, A., Boers, R., Boucher, O., de Leeuw, G., Denier van der Gon, H. A. C., Feichter, J., Krejci, R., Laj, P., Lihavainen, H., Lohmann, U., McFiggans, G., Mentel, T., Pilinis, C., Riipinen, I., Schulz, M., Stohl, A., Swietlicki, E., Vignati, E., Alves, C., Amann, M., Ammann, M., Arabas, S., Artaxo, P., Baars, H., Beddows, D. C. S., Bergström, R., Beukes, J. P., Bilde, M., Burkhart, J. F., Canonaco, F., Clegg, S. L., Coe, H., Crumeyrolle, S., D'Anna, B., Decesari, S., Gilardoni, S., Fischer, M., Fjaeraa, A. M., Fountoukis, C., George, C., Gomes, L., Halloran, P., Hamburger, T., Harrison, R. M., Herrmann, H., Hoffmann, T., Hoose, C., Hu, M., Hyvärinen, A., Hõrrak, U., Iinuma, Y., Iversen, T., Josipovic, M., Kanakidou, M., Kiendler-Scharr, A., Kirkevåg, A., Kiss, G., Klimont, Z., Kolmonen, P., Komppula, M., Kristjánsson, J.-E., Laakso, L., Laaksonen, A., Labonnote, L., Lanz, V. A., Lehtinen, K. E. J., Rizzo, L. V., Makkonen, R., Manninen, H. E., McMeeking, G., Merikanto, J., Minikin, A., Mirme, S., Morgan, W. T., Nemitz, E., O'Donnell, D., Panwar, T. S., Pawlowska, H., Petzold, A., Pienaar, J. J., Pio, C., Plass-Duelmer, C., Prévôt, A. S. H., Pryor, S., Reddington, C. L., Roberts, G., Rosenfeld, D., Schwarz, J., Seland, Ø., Sellegri, K., Shen, X. J., Shiraiwa, M., Siebert, H., Sierau, B., Simpson, D., Sun, J. Y., Topping, D., Tunved, P., Vaattovaara, P., Vakkari, V., Veefkind, J. P., Visschedijk, A., Vuollekoski, H., Vuolo, R., Wehner, B., Wildt, J., Woodward, S., Worsnop, D. R., van Zadelhoff, G.-J., Zardini, A. A., Zhang, K., van Zyl, P. G., Kerminen, V.-M., S. Carslaw, K., and Pandis, S. N.: General overview: European Integrated project on Aerosol Cloud Climate and Air Quality interactions (EUCAARI) – integrating aerosol research from nano to global scales, Atmos. Chem. Phys., 11, 13061–13143, doi:10.5194/acp-11-13061-2011, 2011.

Kulmala, M., Petäjä, T., Nieminen, T., Sipilä, M., Manninen, H. E., Lehtipalo, K., Dal Maso, M., Aalto, P. P., Junninen, H., Paasonen, P., Riipinen, I., Lehtinen, K. E. J., Laaksonen, A., and Kerminen, V.-M.: Measurement of the nucleation of atmospheric aerosol particles, Nat. Protoc., 7, 1651–1667, 2012.

Lohmann, U. and Feichter, J.: Global indirect aerosol effects: a review, Atmos. Chem. Phys., 5, 715–737, doi:10.5194/acp-5-715-2005, 2005.

Manninen, H. E., Nieminen, T., Asmi, E., Gagné, S., Häkkinen, S., Lehtipalo, K., Aalto, P., Vana, M., Mirme, A., Mirme, S., Hõrrak, U., Plass-Dülmer, C., Stange, G., Kiss, G., Hoffer, A., Törő, N., Moerman, M., Henzing, B., de Leeuw, G., Brinkenberg, M., Kouvarakis, G. N., Bougiatioti, A., Mihalopoulos, N., O'Dowd, C., Ceburnis, D., Arneth, A., Svenningsson, B., Swietlicki, E., Tarozzi, L., Decesari, S., Facchini, M. C., Birmili, W., Sonntag, A., Wieden-

Title Page

Abstract | Introduction

Conclusions | References

Tables | Figures

|◄ | ►|

◄ | ►

Back | Close

Full Screen / Esc

Printer-friendly Version

Interactive Discussion

sohler, A., Boulon, J., Sellegri, K., Laj, P., Gysel, M., Bukowiecki, N., Weingartner, E., Wehrle, G., Laaksonen, A., Hamed, A., Joutsensaari, J., Petäjä, T., Kerminen, V.-M., and Kulmala, M.: EUCAARI ion spectrometer measurements at 12 European sites – analysis of new particle formation events, Atmos. Chem. Phys., 10, 7907–7927, doi:10.5194/acp-10-7907-2010, 2010.

Manninen, H. E., Franchin, A., Schobesberger, S., Hirsikko, A., Hakala, J., Skromulis, A., Kangasluoma, J., Ehn, M., Junninen, H., Mirme, A., Mirme, S., Sipilä, M., Petäjä, T., Worsnop, D. R., and Kulmala, M.: Characterisation of corona-generated ions used in a Neutral cluster and Air Ion Spectrometer (NAIS), Atmos. Meas. Tech., 4, 2767–2776, doi:10.5194/amt-4-2767-2011, 2011.

Mikkonen, S., Romakkaniemi, S., Smith, J. N., Korhonen, H., Petäjä, T., Plass-Duelmer, C., Boy, M., McMurry, P. H., Lehtinen, K. E. J., Joutsensaari, J., Hamed, A., Mauldin III, R. L., Birmili, W., Spindler, G., Arnold, F., Kulmala, M., and Laaksonen, A.: A statistical proxy for sulphuric acid concentration, Atmos. Chem. Phys., 11, 11319–11334, doi:10.5194/acp-11-11319-2011, 2011.

Mirme, S. and Mirme, A.: The mathematical principles and design of the NAIS – a spectrometer for the measurement of cluster ion and nanometer aerosol size distributions, Atmos. Meas. Tech., 6, 1061–1071, doi:10.5194/amt-6-1061-2013, 2013.

Napari, I., Noppel, M., Vehkamäki, H., and Kulmala, M.: Parametrization of ternary nucleation rates for H_2SO_4-NH3-H2O vapors, J. Geophys. Res., 107, 4381, doi:10.1029/2002JD002132, 2002.

Nilsson, E. D., Rannik, Ü., Kulmala, M., Buzorius, G., and O'Dowd, C. D.: Effects of continental boundary layer evolution, convection, turbulence and entrainment, on aerosol formation, Tellus B, 53, 4, 441–461, 2001.

Paasonen, P., Nieminen, T., Asmi, E., Manninen, H. E., Petäjä, T., Plass-Dülmer, C., Flentje, H., Birmili, W., Wiedensohler, A., Hõrrak, U., Metzger, A., Hamed, A., Laaksonen, A., Facchini, M. C., Kerminen, V.-M., and Kulmala, M.: On the roles of sulphuric acid and low-volatility organic vapours in the initial steps of atmospheric new particle formation, Atmos. Chem. Phys., 10, 11223–11242, doi:10.5194/acp-10-11223-2010, 2010.

Petäjä, T., Mauldin, III, R. L., Kosciuch, E., McGrath, J., Nieminen, T., Paasonen, P., Boy, M., Adamov, A., Kotiaho, T., and Kulmala, M.: Sulfuric acid and OH concentrations in a boreal forest site, Atmos. Chem. Phys., 9, 7435–7448, doi:10.5194/acp-9-7435-2009, 2009.

Title Page

Abstract | Introduction

Conclusions | References

Tables | Figures

|◄ | ►|

◄ | ►

Back | Close

Full Screen / Esc

Printer-friendly Version

Interactive Discussion

Pirjola, L., Kulmala, M., Wilck, M., Bischoff, A., Stratmann, F., and Otto, E.: Formation of sulphuric acid aerosols and cloud condensation nuclei: an expression for significant nucleation and model comprarison, J. Aerosol Sci., 30, 1079–1094, 1999.

Pope, C. A. and Dockery, D. W.: Health effects of fine particulate air pollution: lines that connect, J. Air Waste Manage., 56, 709–742, 2006.

Poulain, L., Spindler, G., Birmili, W., Plass-Dülmer, C., Wiedensohler, A., and Herrmann, H.: Seasonal and diurnal variations of particulate nitrate and organic matter at the IfT research station Melpitz, Atmos. Chem. Phys., 11, 12579–12599, doi:10.5194/acp-11-12579-2011, 2011.

Riccobono, F., Schobesberger, S., Scott, C. E., Dommen, J., Ortega, I. K., Rondo, L., Almeida, J., Amorim, A., Bianchi, F., Breitenlechner, M., David, A., Downard, A., Dunne, E. M., Duplissy, J., Ehrhart, S., Flagan, R. C., Franchin, A., Hansel, A., Junninen, H., Kajos, M., Keskinen, H., Kupc, A., Kürten, A., Kvashin, A. N., Laaksonen, A., Lehtipalo, K., Makhmutov, V., Mathot, S., Nieminen, T., Onnela, A., Petäjä, T., Praplan, A. P., Santos, F. D., Schallhart, S., Seinfeld, J. H., Sipilä, M., Spracklen, D. V., Stozhkov, Y., Stratmann, F., Tomé, A., Tsagkogeorgas, G., Vaattovaara, P., Viisanen, Y., Vrtala, A., Wagner, P. E., Weingartner, E., Wex, H., Wimmer, D., Carslaw, K. S., Curtius, J., Donahue, N. M., Kirkby, J., Kulmala, M., Worsnop, D. R., and Baltensperger, U.: Oxidation products of biogenic emissions contribute to nucleation of atmospheric particles, Science, 344, 717–721, 2014.

Riipinen, I., Pierce, J. R., Yli-Juuti, T., Nieminen, T., Häkkinen, S., Ehn, M., Junninen, H., Lehtipalo, K., Petäjä, T., Slowik, J., Chang, R., Shantz, N. C., Abbatt, J., Leaitch, W. R., Kerminen, V.-M., Worsnop, D. R., Pandis, S. N., Donahue, N. M., and Kulmala, M.: Organic condensation: a vital link connecting aerosol formation to cloud condensation nuclei (CCN) concentrations, Atmos. Chem. Phys., 11, 3865–3878, doi:10.5194/acp-11-3865-2011, 2011.

Rohrer, F. and Berresheim, H.: Strong correlation between levels of tropospheric hydroxyl radicals and solar ultraviolet radiation, Nature, 442, 184–187, 2006.

Schobesberger, S., Franchin, A., Bianchi, F., Rondo, L., Duplissy, J., Kürten, A., Ortega, I. K., Metzger, A., Schnitzhofer, R., Almeida, J., Amorim, A., Dommen, J., Dunne, E. M., Ehn, M., Gagné, S., Ickes, L., Junninen, H., Hansel, A., Kerminen, V.-M., Kirkby, J., Kupc, A., Laaksonen, A., Lehtipalo, K., Mathot, S., Onnela, A., Petäjä, T., Riccobono, F., Santos, F. D., Sipilä, M., Tomé, A., Tsagkogeorgas, G., Viisanen, Y., Wagner, P. E., Wimmer, D., Curtius, J., Donahue, N. M., Baltensperger, U., Kulmala, M., and Worsnop, D. R.: On the composition of

Title Page

Abstract | Introduction

Conclusions | References

Tables | Figures

|◄ | ►|

◄ | ►

Back | Close

Full Screen / Esc

Printer-friendly Version

Interactive Discussion

ammonia–sulfuric-acid ion clusters during aerosol particle formation, Atmos. Chem. Phys., 15, 55–78, doi:10.5194/acp-15-55-2015, 2015.

Sipilä, M., Berndt, T., Petäjä, T., Brus, D., Vanhanen, J., Stratmann, F., Patokoski, J., Mauldin III, R. L., Hyvärinen, A.-P., Lihavainen, H., and Kulmala, M.: Role of sulfuric acid in atmospheric nucleation, Science, 327, 1243–1246, 2010.

Sipilä, M., Lehtipalo, K., and Kulmala, M.: Atmospheric particle nucleation, in: Aerosol Science – Technology and applications, edited by: Colbeck, I. and Lazaridis, M., John Wiley and Sons, Chichester, UK, 153–180, 2014.

Spindler, G., Mölders, N., Hanss, J., Beier, N., and Kramm, G.: Determining the dry deposition of SO_2, O_3, NO, and NO_2 at the SANA core station Melpitz, Meteorolog. Z., 5, 205–220, 1996.

Spindler, G., Brüggemann, E., Gnauk, T., Grüner, A., Müller, K., and Herrmann, H.: A four-year size-segregated characterization study of particles PM_{10}, $PM_{2.5}$ and PM_1 depending on air mass origin at Melpitz, Atmos. Environ., 44, 164–173, 2010.

Spracklen, D. V., Carslaw, K. S., Merikanto, J., Mann, G. W., Reddington, C. L., Pickering, S., Ogren, J. A., Andrews, E., Baltensperger, U., Weingartner, E., Boy, M., Kulmala, M., Laakso, L., Lihavainen, H., Kivekäs, N., Komppula, M., Mihalopoulos, N., Kouvarakis, G., Jennings, S. G., O'Dowd, C., Birmili, W., Wiedensohler, A., Weller, R., Gras, J., Laj, P., Sellegri, K., Bonn, B., Krejci, R., Laaksonen, A., Hamed, A., Minikin, A., Harrison, R. M., Talbot, R., and Sun, J.: Explaining global surface aerosol number concentrations in terms of primary emissions and particle formation, Atmos. Chem. Phys., 10, 4775–4793, doi:10.5194/acp-10-4775-2010, 2010.

Stratmann, F., Siebert, H., Spindler, G., Wehner, B., Althausen, D., Heintzenberg, J., Hellmuth, O., Rinke, R., Schmieder, U., Seidel, C., Tuch, T., Uhrner, U., Wiedensohler, A., Wandinger, U., Wendisch, M., Schell, D., and Stohl, A.: New-particle formation events in a continental boundary layer: first results from the SATURN experiment, Atmos. Chem. Phys., 3, 1445–1459, doi:10.5194/acp-3-1445-2003, 2003.

Tuch, T. M., Haudek, A., Müller, T., Nowak, A., Wex, H., and Wiedensohler, A.: Design and performance of an automatic regenerating adsorption aerosol dryer for continuous operation at monitoring sites, Atmos. Meas. Tech., 2, 417–422, doi:10.5194/amt-2-417-2009, 2009.

Weber, R. J., McMurry, P. H., Mauldin III, R. L., Tanner, D. J., Eisele, F. L., Clarke, A. D., and Kapustin, V. N.: New particle formation in the remote troposphere: a comparison of observations at various sites, Geophys. Res. Lett., 26, 307–310, 1999.

Title Page

Abstract | Introduction

Conclusions | References

Tables | Figures

◄ | ►

◄ | ►

Back | Close

Full Screen / Esc

Printer-friendly Version

Interactive Discussion

Wehner, B., Petäjä, T., Boy, M., Engler, C., Birmili, W., Tuch, T., Wiedensohler, A., and Kulmala, M.: The contribution of sulfuric acid and non-volatile compounds on the growth of freshly formed atmospheric aerosols, Geophys. Res. Lett., 32, L17810, doi:10.1029/2005GL023827, 2005.

5 Wiedensohler, A., Birmili, W., Nowak, A., Sonntag, A., Weinhold, K., Merkel, M., Wehner, B., Tuch, T., Pfeifer, S., Fiebig, M., Fjäraa, A. M., Asmi, E., Sellegri, K., Depuy, R., Venzac, H., Villani, P., Laj, P., Aalto, P., Ogren, J. A., Swietlicki, E., Williams, P., Roldin, P., Quincey, P., Hüglin, C., Fierz-Schmidhauser, R., Gysel, M., Weingartner, E., Riccobono, F., Santos, S., Grüning, C., Faloon, K., Beddows, D., Harrison, R., Monahan, C., Jennings, S. G.,
10 O'Dowd, C. D., Marinoni, A., Horn, H.-G., Keck, L., Jiang, J., Scheckman, J., McMurry, P. H., Deng, Z., Zhao, C. S., Moerman, M., Henzing, B., de Leeuw, G., Löschau, G., and Bastian, S.: Mobility particle size spectrometers: harmonization of technical standards and data structure to facilitate high quality long-term observations of atmospheric particle number size distributions, Atmos. Meas. Tech., 5, 657–685, doi:10.5194/amt-5-657-2012, 2012.

15 Yu, F. and Turco, R. P.: The size-dependent charge fraction of sub-3-nm particles as a key diagnostic of competitive nucleation mechanisms under atmospheric conditions, Atmos. Chem. Phys., 11, 9451–9463, doi:10.5194/acp-11-9451-2011, 2011.

Zieger, P., Fierz-Schmidhauser, R., Poulain, L., Müller, T., Birmili, W., Spindler, G., Wiedensohler, A., Baltensperger, U., and Weingartner, E.: Influence of water uptake on the aerosol
20 particle light scattering coefficients of the Central European aerosol, Tellus B, 66, 22716, doi:10.3402/tellusb.v66.22716, 2014.

Title Page

Abstract | Introduction

Conclusions | References

Tables | Figures

|◄ | ►|

◄ | ►

Back | Close

Full Screen / Esc

Printer-friendly Version

Interactive Discussion

Table 1. Data coverage during the four measurement periods 2008–2011. The list contains the number of days for which a complete diurnal cycle of NAIS data was available. Further columns indicate additional availability of other parameters. Also, the serial number of the used NAIS instrument is indicated.

Period name	Duration	NAIS S/N	Days with complete availability of . . . data			
			NAIS	+TDMPS-APS	+ H_2SO_4	+NH_3
Period I	1 May 2008–07 January 2009	4	199	121	55	0
Period II	26 March 2009–05 August 2009	4	78	28	28	0
Period III	3 June 2010–18 October 2010	15	129	53	53	32
Period IV	10 March 2011–17 October 2011	15	203	99	89	88

Table 2. Classification of NPF events according to their CI peak and two specific threshold values based on complete NAIS-TDMPS data set.

Class Name	Description	CI_{max} Range [$s\,cm^{-6}$]	No. of days	Average time of peak $N_{[2;20\,nm]}$
Class I	Events with highest NPF intensity	$CI_{max} \geq 3 \times 10^8$	97	11:34 CET
Class II	Events with intermediate NPF intensity	$7 \times 10^7 \leq CI_{max} < 3 \times 10^8$	99	12:26 CET
Class III	Events with low NPF intensity including "non-events"	$7 \times 10^7 < CI_{max}$	93	11:05 CET

Table A1. List of 27 manually selected NPF event days whose average diurnal profiles of $N_{(2-20)}$ served as a reference function $f(t)$ in Eq. (3). This list encompasses NPF events that showed clear patterns of particle nucleation and subsequent growth in terms of particle number size distributions.

Date	Peak value of $N_{(2-20)}$ in cm^{-3}
7 May 2008	218 181
11 May 2008	102 548
14 May 2008	115 326
19 May 2008	43 778
29 May 2008	69 170
30 May 2008	7411
5 June 2008	119 236
6 June 2008	58 621
7 June 2008	58 384
3 July 2008	31 699
6 August 2008	243 303
31 August 2008	127 456
2 April 2009	63 281
3 April 2009	133 927
25 April 2009	279 349
2 May 2009	71 389
13 June 2010	19 583
17 June 2010	93 611
19 June 2010	74 563
20 July 2010	80 346
25 July 2010	18 250
27 March 2011	54 071
5 May 2011	24 497
10 May 2011	137 736
17 June 2011	111 979
7 July 2011	15 041
17 August 2011	111 657

Table A2. Comparison of two classification schemes for new particle formation events: the CI method (Class I, Class II and Class III; cf. Table 2) and the University of Helsinki (UHEL) classification, originally reported in Dal Maso et al. (2005).

CI method	UHELclass 1a	UHELclass 1b	UHELclass 2	UHELnon-event	Total
I	36	33	22	1	92
II	14	29	29	10	82
III	0	9	16	64	89
Total	50	71	67	75	263

Figure 1. Establishing proximity measures based on experimental correlations determined during the EUCAARI 2008 campaign. **(a)** [·OH], through correlation analysis of experimental values with the global radiation flux **(b)** [H_2SO_4], through correlation between experimental H_2SO_4 values and calculated [·OH] combined with measured [SO_2] and calculated CS.
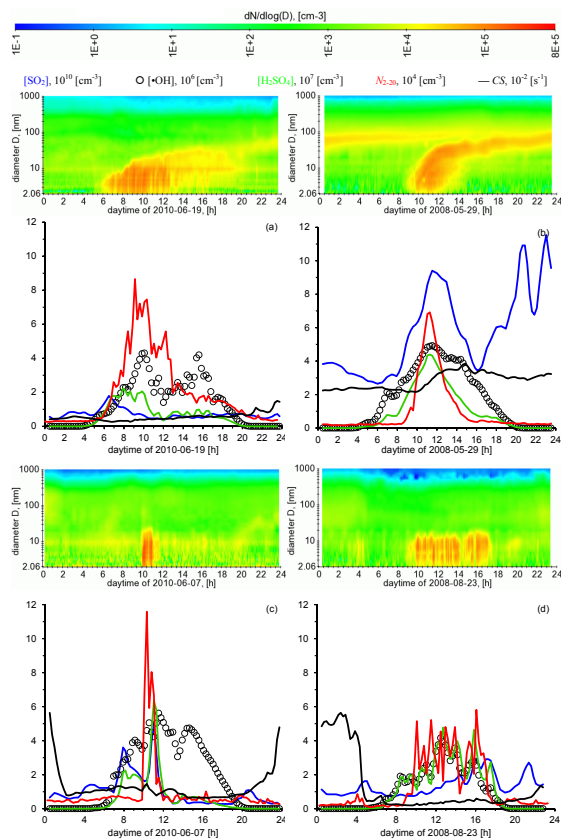
Figure 2. Diurnal time series of the particle number size distribution, concentration of sulfur dioxide SO_2, hydroxyl radicals $\cdot OH$ and sulfuric acid H_2SO_4, ultrafine particle number concentration N_{2-20} and condensational sink CS for 4 cases: **(a)** 19 June 2010, **(b)** 29 May 2008, **(c)** 7 June 2010, **(d)** 23 August 2008.
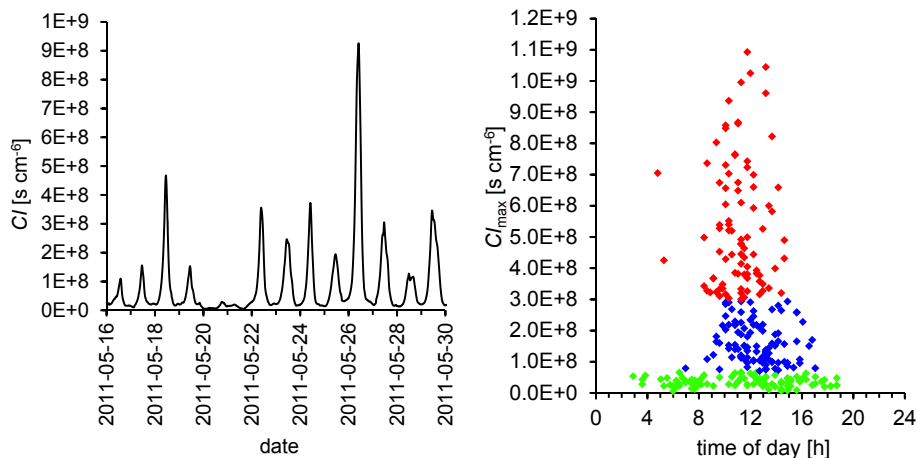
Figure 3. Left: exemplary time series of the convolution integral CI from 16–30 May 2011, indicating the intensity of new particle formation. Right: daily maximum of the convolution integral CI for all observation days as a function of time of day of that maximum. Event classes were subsequently defined class I (red, intense new particle formation), class II (blue, new particle formation at lower intensity), and class III (green, NPF below significance level). Cf. Table 2 for the threshold values of CI used for this classification.
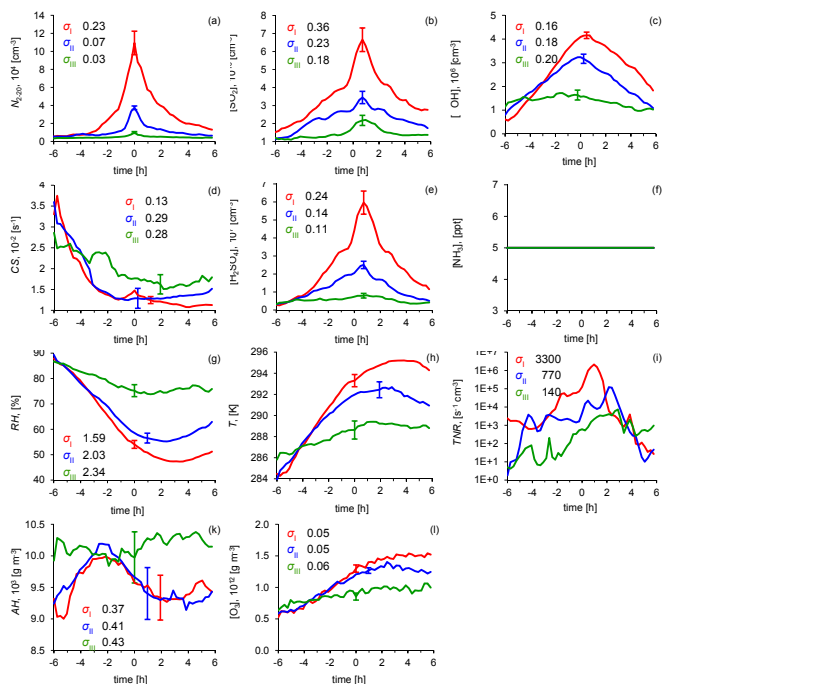
Figure 4. Time series of atmospheric parameters for the three NPF event classes, red = Class I event, blue = Class II event, green = Class III (weak events and "non-events"). The subfigures show concentrations of **(a)** ultrafine particles (N_{2-20}), **(b)** sulphur dioxide (SO_2) and **(c)** hydroxyl radicals (·OH), **(d)** the condensational sink (CS), the concentrations of **(e)** sulphuric acid (H_2SO_4) and **(f)** ammonia (NH_3 = 5 ppt), **(g)** the relative humidity (RH), **(h)** the temperature (T), **(i)** ternary nucleation rates (TNR) under assumption of a constant ammonia concentration [NH_3] = 5 ppt, **(j)** the absolute humidity (AH) and ozone (O_3) for 3 Event Classes. Whiskers indicate one SD. Data coverage: Class I (55 days), Class II (60 days), Class III (67 days). The arithmetic mean event peak times were: Class I (10:48 LT), Class II (11:54 LT), Class III (11:46 LT).
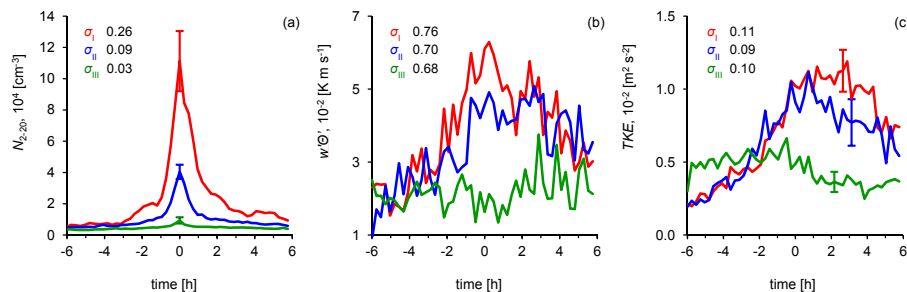
Figure 5. Time series of **(a)** the concentrations of ultrafine particles (N_{2-20}), **(b)** the vertical turbulent heat flux ($w'\theta'$) and **(c)** turbulent kinetic energy (TKE) for the year 2010 and 3 Event Classes (red = Class I event, blue = Class II event, green = Class III including weak events and "non-events"). Whiskers indicate one SD. Data coverage: Class I (19 days), Class II (17 days), Class III (27 days).
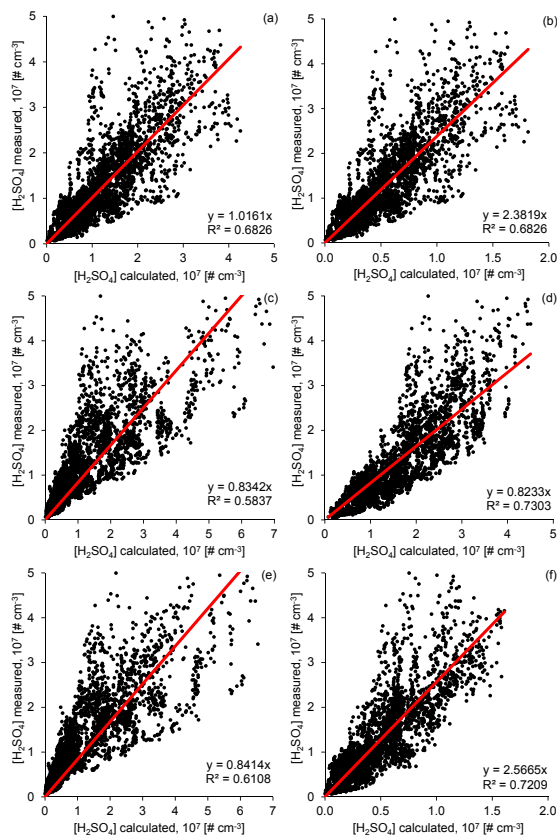
Figure A1. Extended version of Fig. 1, illustrating expressions for the [H$_2$SO$_4$] proxy from Mikkonnen et al., 2011: **(a)** Eq. (4) with Eq. (3), **(b)** L1, **(c)** L2, **(d)** L3, **(e)** L4, **(f)** L5. Data refer to 9 days during the EUCAARI campaign in 2008.

Full Screen / Esc

Printer-friendly Version

Interactive Discussion
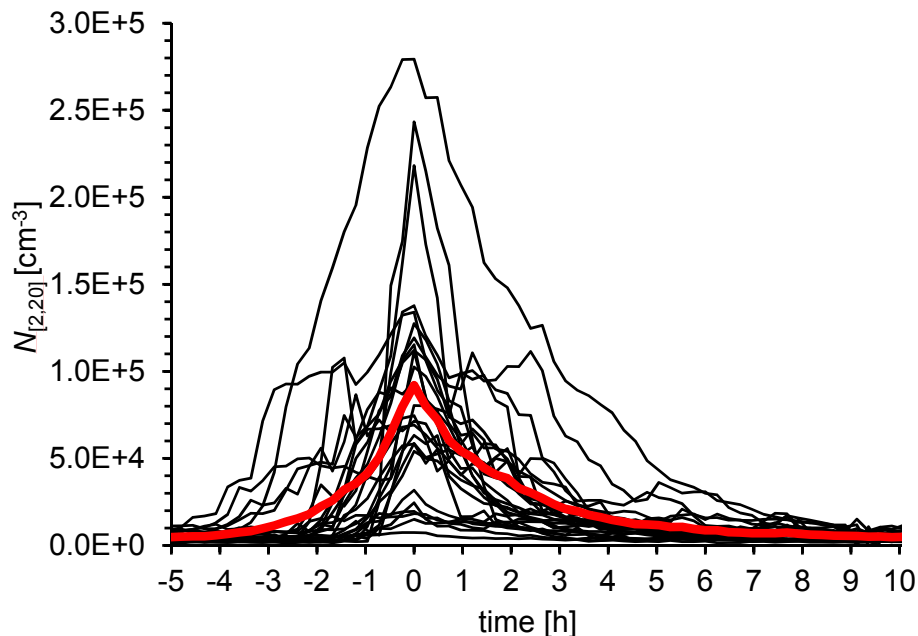
Figure A2. Time series of $N_{[2;20]}$ for the 27 manually selected NPF events listed in Table A1. The red curve indicates the arithmetic average of the time series, which are shifted so that they coincide in maximum number concentration.
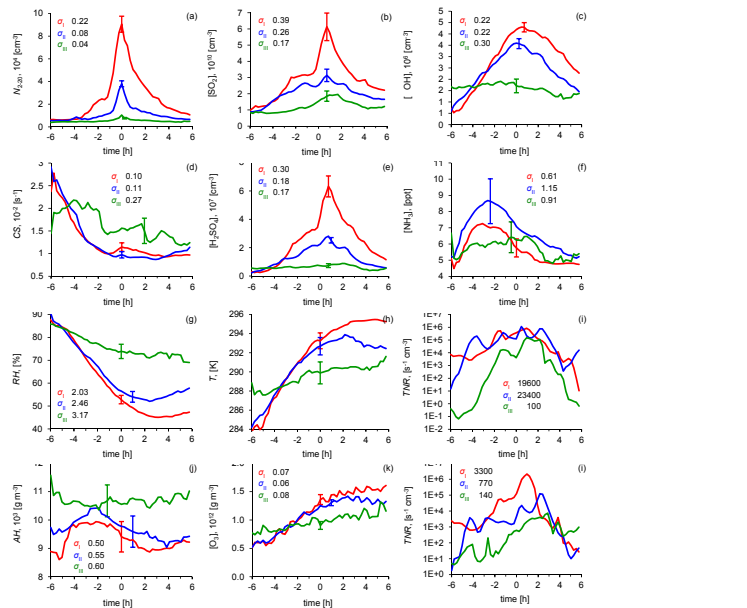
Figure A3. Alternative version to Fig. 4, however, limited to the years 2010–2011 when experimental ammonia concentrations were available. The graphs show time series of atmospheric parameters for the three NPF event classes, red = Class I event, blue = Class II event, green = Class III even, including weak events and "non-events". The subfigures show concentrations of **(a)** ultrafine particles (N_{2-20}), **(b)** sulphur dioxide (SO_2) and **(c)** hydroxyl radicals ($\cdot OH$), **(d)** the condensational sink (CS), the concentrations of **(e)** sulphuric acid (H_2SO_4) and **(f)** ammonia (NH_3), **(g)** the relative humidity (RH), **(h)** the temperature (T), **(i)** ternary nucleation rates (TNR), **(j)** the absolute humidity (AH) and ozone (O_3) for 3 Event Classes for time ranges, when measured ammonia concentrations are available. **(l)** represents the estimated ternary nucleation rate (TNR*) according to Napari et al. (2002). Whiskers indicate one SD. Data coverage: Class I (33 days), Class II (35 days), Class III (40 days). The arithmetic mean event peak times were: Class I (10:48 LT), Class II (11:54 LT), Class III (11:46 LT).
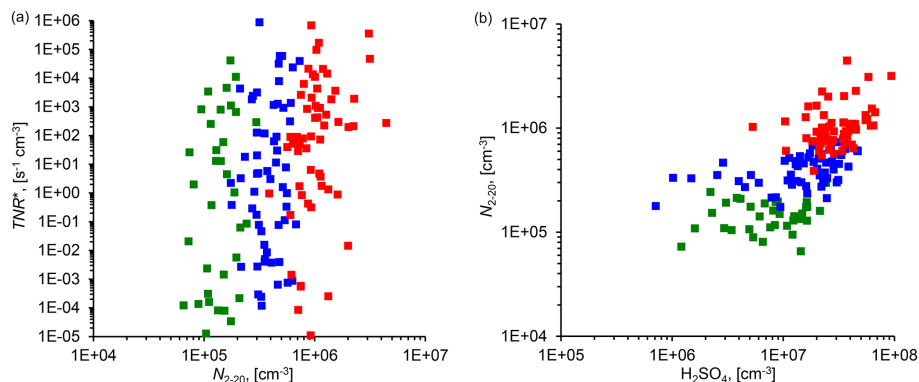
Figure A4. (a) Correlation between the ternary nucleation rate (TNR*, with $NH_3 = 5$ ppt) and ultrafine particle number concentration ($N_{2–20}$). Colours refer to event class Class I (red), Class II (blue), and Class III (green). **(b)** Correlation between the particle number concentration $N_{[2–20]}$ and the calculated sulphuric acid concentration $[H_2SO_4]$ in this work. Colours refer to event class Class I (red), Class II (blue), and Class III (green).
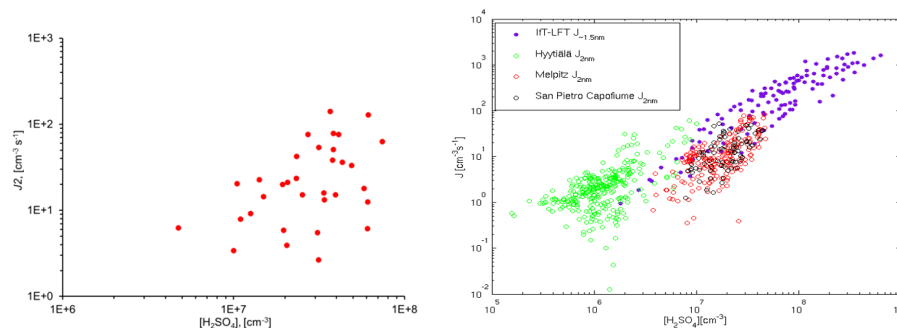
Figure A5. Left: correlation between the particle formation rate J_2 and the calculated sulphuric acid concentration $[H_2SO_4]$ in this work. The diagram involves 33 cases of NPF events between 2008 and 2011. Right: the same relationship from Kerminen et al. (2010).